

UNIVERSIDADE ESTADUAL DE CAMPINAS
SISTEMA DE BIBLIOTECAS DA UNICAMP
REPOSITÓRIO DA PRODUÇÃO CIENTÍFICA E INTELLECTUAL DA UNICAMP

Versão do arquivo anexado / Version of attached file:

Versão do Editor / Published Version

Mais informações no site da editora / Further information on publisher's website:

<https://journals.aps.org/prb/abstract/10.1103/PhysRevB.85.195110>

DOI: 10.1103/PhysRevB.85.195110

Direitos autorais / Publisher's copyright statement:

©2012 by American Physical Society. All rights reserved.

DIRETORIA DE TRATAMENTO DA INFORMAÇÃO

Cidade Universitária Zeferino Vaz Barão Geraldo

CEP 13083-970 – Campinas SP

Fone: (19) 3521-6493

<http://www.repositorio.unicamp.br>

Suppression of Anderson localization of light in one-dimensional disordered photonic superlatticesE. Reyes-Gómez,¹ A. Bruno-Alfonso,² S. B. Cavalcanti,³ and L. E. Oliveira⁴¹*Instituto de Física, Universidad de Antioquia, AA 1226, Medellín, Colombia*²*Faculdade de Ciências, UNESP-Universidade Estadual Paulista, 17033-360, Bauru-SP, Brazil*³*Instituto de Física, Universidade Federal de Alagoas, Maceió-AL, 57072-970, Brazil*⁴*Instituto de Física, Universidade Estadual de Campinas-UNICAMP, Campinas-SP, 13083-859, Brazil*

(Received 2 February 2012; published 7 May 2012)

The localization properties of electromagnetic modes in one-dimensional disordered photonic superlattices are theoretically studied. The multilayered system is considered to be composed of alternating stacks of two different random-thickness slabs, characterized by nondispersive and/or frequency-dependent electric permittivities and magnetic permeabilities. Results for the localization length are evaluated by using an analytical model for weakly disordered systems as well as its general definition through the transmissivity properties of the heterostructure. Good agreement between both results is observed only for small amplitudes of disorder. The critical frequencies at which the localization length diverges are correctly predicted in the whole frequency spectrum by the analytical model and confirmed via the corresponding numerical calculations. The λ^2 dependence of the localization length, previously observed in disordered heterostructures made of material of positive refractive indexes, are confirmed in the present work. In addition, new λ^4 and λ^{-4} dependencies of the localization length in positive-negative disordered photonic superlattices are obtained, under certain specific conditions, in the long and short wavelength limits, respectively. The asymptotic behavior of the localization length in these limits is essentially determined by the particular frequency dispersion that characterizes the metamaterial used in the left-handed layers. When the effects of absorption are considered, then a divergence of the localization length is still observed, under some conditions, in the short wavelength limit.

DOI: [10.1103/PhysRevB.85.195110](https://doi.org/10.1103/PhysRevB.85.195110)

PACS number(s): 78.67.Pt, 42.25.Dd, 72.15.Rn

I. INTRODUCTION

The complex and fascinating physics behind Anderson localization¹ has stimulated a rich variety of theoretical and experimental work, worldwide, on the nature of wave propagation in random media. Characterized originally by the vanishing of the electronic diffusion in disordered media, this interference wave phenomenon has been investigated in all sorts of waves, from electromagnetic to seismic ones. Anderson localization has been observed in classical wave systems such as microwave, light, and ultrasound.² The vectorial character of the electromagnetic waves may provide interesting phenomena not known in their electronic counterpart. The microstructuring techniques of high-quality optical materials, available nowadays, have given a new thrust to develop further studies on this important and puzzling phenomenon. Disorder and localization effects on light propagation in photonic crystals (PC) have been investigated both theoretically and experimentally.^{3,4} Due to the remarkable flexibility in the fabrication of new materials, one is able to tailor the electromagnetic dispersion relation and mode structure of a material to suit almost any need,⁵ such as the simultaneous negative electric permittivity and magnetic permeability of a so-called metamaterial or a left-handed material (LHM) in contrast with the usual right-handed material (RHM), an allusion to the vectorial product between the electric and magnetic fields.⁶ To ensure positiveness of the electromagnetic energy density,⁷ a LHM must be dispersive. Furthermore, it exhibits optical magnetism.^{8,9} This particular feature induces new possibilities for the control of light propagation, such as negative refraction, superlens, and cloaking.^{10–12} A study on a one-dimensional (1D) structure composed of alternate layers of air and a nondispersive LHM, where the disorder was introduced by

randomizing the refractive indices of the layers, has indicated strong suppression of Anderson localization^{13,14} and unusual behavior of the localization length ξ at long wavelengths λ , in contrast with the well-known $\xi \propto \lambda^2$ asymptotic behavior.¹⁵ Although in Refs. 13 and 14 it was shown that $\xi \propto \lambda^6$, this result is essentially due to the insufficient size of the systems considered in the numerical calculations, and a recent analytical study¹⁶ indicated that, in such systems, the correct asymptotic behavior of the localization length is $\xi \propto \lambda^8$.

An interesting example of the impact of optical magnetism is given by the observation of Brewster angles in a transversal-electric (TE) configuration of the electromagnetic field propagating through a LHM, evidencing the role played by the magnetic dipoles in the polarization of light. The influence of a dispersive electromagnetic response on Anderson localization in a long stack assembled by alternating a pair of materials, a dispersive one (right or left handed) and a right-handed nondispersive one, has been thoroughly investigated illustrating interesting new features that appears due to a combination of oblique incidence and dispersion.^{17–20} By choosing incident light through 1D disordered structures at Brewster angles, one finds a polarization-induced delocalization effect.²¹ Indeed, for specific combinations of angle of incidence and frequency, Brewster anomalies are present (for both states of polarization and not necessarily within the negative-refraction regime), thus effectively delocalizing light. It was also found that the power-of- λ asymptotic behavior of the localization length does not hold for large angles of incidence. Furthermore, by taking into account correlations effects, one finds that these do not modify the asymptotic behavior of the localization length although absorption tends to suppress the delocalized Brewster modes.¹⁸ Investigations on a RHM-LHM Fibonacci heterostructure

have illustrated the influence of the combination dispersion-quasiperiodicity on the localization length.¹⁹ The effects of the absorption on the Anderson localization of electromagnetic waves in weakly disordered systems were also theoretically investigated.²⁰ Such studies reveal that delocalized modes, obtained from numerical simulations in nonabsorptive media, are gradually suppressed as the absorption level is increased.

In the present work, we set out to investigate the influence of the particular medium response on the localization length of 1D stacks composed of nondispersive RHM-RHM or RHM-LHM superlattices, in which the LHM layer is considered dispersive, in order to understand the behavior of the localization length under various types of medium responses. This paper is organized as follows: In Sec. II the theoretical procedure is described. In Sec. III we show the results obtained for various types of heterostructures: a nondispersive RHM-RHM superlattice, a RHM-LHM superlattice in which the LHM is characterized by Drude-type responses, and, finally, a RHM-LHM superlattice with the LHM characterized by a dispersive split-ring resonator (SRR) electric permittivity and magnetic permeability, with and without absorption effects. Section IV presents our conclusions that amounts to say that the asymptotic behavior of the localization length depends crucially on the particular medium response.

II. THEORETICAL FRAMEWORK

Here we consider a multilayered system composed of alternating stacks of two different slabs of optical materials A and B , which are characterized by electric permittivities and magnetic permeabilities ϵ_A and μ_A , and ϵ_B and μ_B , respectively. The multilayered system under consideration is supposed to be sandwiched between two semi-infinite layers of material A . The width a_j (b_j) of the layer A (B) at the j th site of the multilayered system is defined as $a_j = a + \delta_j^A$ ($b_j = b + \delta_j^B$), where δ_j^A (δ_j^B) are random variables uniformly distributed in the interval $[-\Delta_A/2, \Delta_A/2]$ ($[-\Delta_B/2, \Delta_B/2]$). Parameters Δ_A and Δ_B are then the amplitudes of disorder of layers A and B , respectively. Further, we assume that there is no correlation between the disorder of the heterostructure slabs.²² In what follows, the symbol $\langle \dots \rangle$ represents the configurational average of a given geometrical or physical variable, i.e., the average taken over a sufficiently large ensemble of multilayered systems, in which each element of the ensemble corresponds to a system obtained for a single realization of disorder. One may note that $a = \langle a_j \rangle$ and $b = \langle b_j \rangle$.

In order to calculate the localization length of the electromagnetic modes in the multilayered heterostructure, it is, first, necessary to calculate the light-transmission coefficient T of the photonic heterostructure. The transfer-matrix formalism may be used for such purposes.^{17–19} Once the transmission coefficient is obtained for each member of the ensemble, the localization length ξ may be evaluated through the expression^{15,23}

$$\xi^{-1} = - \lim_{N \rightarrow \infty} \left\langle \frac{\ln(T)}{2L} \right\rangle, \quad (1)$$

where N is the number of double layers (AB) in the photonic system and $L = \sum_{j=1}^N (a_j + b_j)$ is the length of the photonic heterostructure. For practical purposes, the limit $N \rightarrow \infty$ in Eq. (1) is reached for a sufficiently large number of layers in each photonic heterostructure of the ensemble over which the configurational average is taken.¹⁹ It is also necessary to explain how the number of elements of such ensemble, i.e., the number of disorder realizations, is chosen. The single-parameter scaling (SPS) principle dictates that $\text{var}(l) = l$, where $\text{var}(l) = \langle l^2 \rangle - \langle l \rangle^2$ is the variance of the dimensionless Lyapunov exponent $l = \langle L \rangle / \xi$, and $\langle L \rangle$ is the average system length.^{24,25} The SPS principle indicates that large values of l lead to large values of the variance $\text{var}(l)$ and, therefore, to large fluctuations of the Lyapunov exponent around its mean value. It then would be important to set up an appropriate value of the number of realizations to take the configurational average. Nevertheless, the SPS principle is violated under some specific conditions and, therefore, it cannot be straightforwardly used to predict the behavior of $\text{var}(l)$ from the value of the Lyapunov exponent.^{24,25} Consequently, an estimation of the optimal number of realizations sufficient to achieve the convergence of Eq. (1) cannot be trivially obtained, by using the SPS principle, from an *a priori* value of the localization length. The number of realizations used in the present paper was chosen by studying the convergence of the localization length, as a function of the number of realizations, for a collection of some frequency values. We noted that, in most of cases discussed below, numerical results for the localization length stabilized around 50–90 realizations of disorder (the study of the convergence will not be shown here).

Although Eq. (1) provides a general way to obtain the localization length in 1D disordered heterostructures, for weakly disordered systems it is possible to derive an analytical expression for ξ in terms of parameters corresponding to a 1D finite photonic crystal without disorder, with slabs A and B of widths a and b , respectively. It has been shown^{17,22} that, in this case, the localization length may be obtained as

$$\xi^{-1} = \frac{K}{8d \sin^2(kd)}, \quad (2)$$

where $d = a + b$, k is the 1D Bloch wave vector in the perfect photonic crystal and

$$K = F_-^2 [Q_A^2 \sigma_A^2 \sin^2(Q_B b) + Q_B^2 \sigma_B^2 \sin^2(Q_A a)]. \quad (3)$$

The variances $\sigma_A^2 = \langle (\delta_j^A)^2 \rangle = \Delta_A^2/12$ and $\sigma_B^2 = \langle (\delta_j^B)^2 \rangle = \Delta_B^2/12$ account for the degrees of disorder of the slabs A and B , respectively, whereas $\sin^2(kd)$ may be computed from the transcendental equation giving the dispersion relation of the periodic 1D photonic crystal, i.e.,

$$\cos(kd) = \cos(Q_A a) \cos(Q_B b) - \frac{1}{2} F_+ \sin(Q_A a) \sin(Q_B b). \quad (4)$$

In the above expressions one has

$$F_{\pm} = \frac{f_A}{f_B} \pm \frac{f_B}{f_A}, \quad (5)$$

where the functions f_x ($x = A, B$), for the TE and TM polarizations, are given by

$$f_x^{\text{TE}} = \frac{u_x}{\mu_x} \quad \text{and} \quad f_x^{\text{TM}} = \frac{u_x}{\epsilon_x}, \quad (6)$$

respectively, $u_x = \sqrt{\epsilon_x \mu_x - \sin^2 \theta}$, $Q_x = (\omega/c)u_x$, and θ is the incidence angle relative to the vacuum. Equation (2) was recently derived by Izrailev and Makarov²² and was generalized by Mogilevtsev *et al.*¹⁷ to include the possibility of oblique incidence. Hereafter we refer to this equation as the Izrailev-Makarov (I-M) equation,²² which was perturbatively obtained under the assumptions that, in the multilayered system, the field phase is homogeneously distributed and the disorder is weak. In other words, the disorder amplitudes should be much less than the mean widths of the slabs composing the heterostructure, and the conditions $Q_x^2 \sigma_x^2 \ll 1$ (with $x = A, B$) should be satisfied²² in order to use Eq. (2). This fact is of particular importance in dispersive superlattices, where the product $Q_x^2 \sigma_x^2$ may be divergent in the limit $\omega \rightarrow 0$, $\omega \rightarrow \infty$ or even at a finite value of the frequency. Therefore, the particular frequency dependencies of both $\epsilon(\omega)$ and $\mu(\omega)$ in each material of the heterostructure will determine the frequency regions where Eq. (2) is applicable.

We now consider the I-M equation in some detail and refer to the localization length as obtained from Eq. (2). We are interested in studying the frequency values at which the localization length diverges, yielding extended states in the disordered multilayered system. We denote such frequency values as ω_c critical frequencies. Of course, ω_c should be real and non-negative. By taking into account Eq. (4), one may note that the inequality

$$|\cos(Q_A a) \cos(Q_B b) - \frac{1}{2} F_+ \sin(Q_A a) \sin(Q_B b)| \leq 1 \quad (7)$$

should be satisfied in the limit $\omega \rightarrow \omega_c$.

We, first, analyze the case of normal incidence ($\theta = 0$), a situation in which one may expect that the condition

$$\lim_{\omega \rightarrow \omega_c} K(\omega) = 0 \quad (8)$$

should be accomplished. In this case ($\theta = 0$), the function K may be written as

$$K(\omega) = \frac{\omega^2}{c^2} g_N(\omega) h_N(\omega), \quad (9)$$

where

$$g_N(\omega) = [\epsilon_A(\omega)\mu_B(\omega) - \epsilon_B(\omega)\mu_A(\omega)]^2 \quad (10)$$

and

$$h_N(\omega) = \sigma_A^2 \frac{\sin^2 \left[\frac{\omega b}{c} \sqrt{\epsilon_B(\omega)\mu_B(\omega)} \right]}{\epsilon_B(\omega)\mu_B(\omega)} + \sigma_B^2 \frac{\sin^2 \left[\frac{\omega a}{c} \sqrt{\epsilon_A(\omega)\mu_A(\omega)} \right]}{\epsilon_A(\omega)\mu_A(\omega)}. \quad (11)$$

If the critical frequencies come from the zeros of g_N , then one may see that $Z_A^2(\omega_c) = Z_B^2(\omega_c)$, where

$$Z_x(\omega) = \frac{\sqrt{\mu_x(\omega)}}{\sqrt{\epsilon_x(\omega)}} \quad (12)$$

is the optical impedance of medium $x = A$ or $x = B$. In other words, the suppression of the Anderson localization would be

due, in this case, to the matching of the square of the optical impedance throughout the multilayered system. As it is known, the impedance matching of two different media leads to the vanishing of the reflectivity at the interface between them,^{22,26} a fact which results in an enhancement of the transmissivity and, as a consequence, in an increase of the localization length. The critical frequencies obtained from the condition $g_N(\omega) = 0$ do not depend on the geometrical parameters or degree of disorder of the multilayered system and are determined by the frequency dependence of the electric permittivities and magnetic permeabilities of slabs A and B .

In the absence of absorption effects, i.e., for electric ϵ_x and magnetic μ_x responses assumed as real functions, a careful analysis of Eq. (11) indicates that the zeros of h_N are not critical frequencies. In fact, the equation $h_N(\omega) = 0$ has no real solutions unless the conditions $\frac{\omega a}{c} \sqrt{\epsilon_A(\omega)\mu_A(\omega)} = m_1 \pi$ and $\frac{\omega b}{c} \sqrt{\epsilon_B(\omega)\mu_B(\omega)} = m_2 \pi$ are simultaneously met for a certain value of the frequency, where m_1 and m_2 are nonzero integer numbers. According to Eq. (4), the above conditions lead to $\cos(kd) = \pm 1$ and, therefore, to the vanishing of $\sin^2(kd)$ in the denominator of Eq. (2). Nevertheless, it is possible to show that the localization length remains finite as the frequency approaches the zeros of h_N .

As the I-M equation was obtained under the condition $Q_x^2 \sigma_x^2 \ll 1$, with $x = A$ and B , one may expect that it would not be valid in a frequency region where the above condition does not hold. However, the I-M equation may still be useful to predict the critical frequencies when $Q_x^2 \sigma_x^2 \gtrsim 1$. The reason is the equivalence between the conditions $g_N(\omega_c) = 0$ and $Z_A^2(\omega_c) = Z_B^2(\omega_c)$ satisfied by the critical frequency in the case of normal incidence: The former one is derived from the I-M equation, whereas the second one is general and independent on the degree of disorder.^{7,22} In this way, apart from the positive real zeros of g_N and the case $\omega = 0$ [cf. Eq. (9)], one has that $\omega \rightarrow \infty$ is a possible candidate to take into account. If $\omega_c = 0$ is a critical frequency, then one may expect a suppression of the Anderson localization in the limit $\lambda \rightarrow \infty$, where $\lambda = 2\pi c/\omega$ is the vacuum wavelength associated with the electromagnetic wave. If $\omega_c \rightarrow \infty$ is a critical frequency, then one may expect a suppression of the Anderson localization in the limit $\lambda \rightarrow 0$. Of course, these frequency values are actual critical frequencies only if condition (7) is satisfied.

A similar reasoning applies for oblique incidence. In this case, the delocalization process is often explained in terms of Brewster anomalies¹⁷⁻¹⁹: If the incidence angle coincides with the Brewster angle θ_B , the reflected electromagnetic wave is suppressed when the incoming monochromatic wave is incident with TM or TE polarization, a fact which gives rise to maximum transmission. In this case the localization length may become larger than the system length and the electromagnetic modes are then delocalized. It is important to stress that, for a given Brewster angle, a set of different frequencies may satisfy the Brewster condition. An important keystone to identify when a critical frequency corresponds to a Brewster anomaly^{17,18} is its strong dependence on θ_B .

For oblique incidence, one may note that K in Eq. (2) is given by

$$K(\omega, \theta) = \frac{\omega^2}{c^2} g_O(\omega, \theta) h_O(\omega, \theta), \quad (13)$$

where

$$h_O(\omega, \theta) = \sigma_A^2 \frac{\sin^2 \left[\frac{\omega b}{c} \sqrt{\epsilon_B(\omega) \mu_B(\omega) - \sin^2 \theta} \right]}{\epsilon_B(\omega) \mu_B(\omega) - \sin^2 \theta} + \sigma_B^2 \frac{\sin^2 \left[\frac{\omega a}{c} \sqrt{\epsilon_A(\omega) \mu_A(\omega) - \sin^2 \theta} \right]}{\epsilon_A(\omega) \mu_A(\omega) - \sin^2 \theta} \quad (14)$$

and g_O is defined for TE and TM modes as

$$g_O^{\text{TE}}(\omega, \theta) = \left[[\epsilon_A(\omega) \mu_A(\omega) - \sin^2 \theta] \frac{\mu_B(\omega)}{\mu_A(\omega)} - [\epsilon_B(\omega) \mu_B(\omega) - \sin^2 \theta] \frac{\mu_A(\omega)}{\mu_B(\omega)} \right]^2 \quad (15)$$

and

$$g_O^{\text{TM}}(\omega, \theta) = \left[[\epsilon_A(\omega) \mu_A(\omega) - \sin^2 \theta] \frac{\epsilon_B(\omega)}{\epsilon_A(\omega)} - [\epsilon_B(\omega) \mu_B(\omega) - \sin^2 \theta] \frac{\epsilon_A(\omega)}{\epsilon_B(\omega)} \right]^2, \quad (16)$$

respectively. For a given value of the Brewster angle θ_B , the critical frequencies should satisfy

$$\lim_{\omega \rightarrow \omega_c} K(\omega, \theta_B) = 0. \quad (17)$$

As in the case of normal incidence, for oblique incidence it is possible to see that, for a given value of the incidence angle θ , the frequency values corresponding to the zeros of $h_O(\omega, \theta)$ are not critical frequencies in the absence of absorption. In this case, the possible candidates to critical frequencies are $\omega = 0$, $\omega \rightarrow \infty$, and the positive real values of ω satisfying equation $g_O^X(\omega, \theta) = 0$, with $X = \text{TE}$ or $X = \text{TM}$.

Frequencies $\omega = 0$ and $\omega \rightarrow \infty$ may be critical frequencies provided that condition (7) is satisfied, that ξ diverges in the limits $\omega \rightarrow 0$ and $\omega \rightarrow \infty$, respectively, and under conditions that we shall discuss below. In any case, $\omega = 0$ and $\omega \rightarrow \infty$ should not be considered as related with Brewster anomalies. In order to expand on this, we suppose that functions ϵ_A , μ_A , ϵ_B , and μ_B have positive finite limits ϵ_A^∞ , μ_A^∞ , ϵ_B^∞ , and μ_B^∞ , respectively, as $\omega \rightarrow \infty$. Moreover, we take $(Z_A^\infty)^2 = (Z_B^\infty)^2$, where Z_A^∞ and Z_B^∞ are the optical impedances of the slabs A and B , respectively, in the high-frequency limit. In this case we expect a suppression of the Anderson localization for normal incidence as $\omega \rightarrow \infty$ due to the matching of the square of the optical impedances of the system at this limit. In addition, if condition $\mu_A^\infty = \mu_B^\infty$ is satisfied, then the function g_O^{TE} becomes independent of θ . This fact, combined with condition $(Z_A^\infty)^2 = (Z_B^\infty)^2$, leads to the vanishing of g_O^{TE} as $\omega \rightarrow \infty$ and, therefore, to the suppression of the Anderson localization for TE modes in the high-frequency region. A similar situation takes place for TM waves. If $\epsilon_A^\infty = \epsilon_B^\infty$, then g_O^{TM} becomes independent of θ and tends toward zero as $\omega \rightarrow \infty$, leading to the suppression of the Anderson localization at this limit. These are cases in which the delocalization process should not be explained in terms of a Brewster anomaly, but one may classify this singularity of ξ as omnidirectional. Furthermore, if $\mu_A^\infty \neq \mu_B^\infty$ ($\epsilon_A^\infty \neq \epsilon_B^\infty$) then the localization of TE (TM) waves occurs for oblique incidence in the high-frequency limit. This analysis may also be extended to the low-frequency region provided that the functions ϵ_A , μ_A , ϵ_B , and μ_B have

finite limits ϵ_A^0 , μ_A^0 , ϵ_B^0 , and μ_B^0 , respectively, as $\omega \rightarrow 0$. Moreover, there may be a physical case in which functions, μ_A , ϵ_A , μ_B , and ϵ_B have positive or negative finite limits μ_A^j , ϵ_A^j , μ_B^j , and ϵ_B^j , respectively, at some finite value ω_j of the wave frequency, and that such value of the frequency satisfies inequality (7). If condition $Z_A^2(\omega_j) = Z_B^2(\omega_j)$ is valid, then ω_j may be a critical frequency for normal incidence. If we also have $\mu_A(\omega_j) = \pm \mu_B(\omega_j)$ [$\epsilon_A(\omega_j) = \pm \epsilon_B(\omega_j)$], then the function $g_O^{\text{TE}}(\omega_j, \theta) = 0$ [$g_O^{\text{TM}}(\omega_j, \theta) = 0$] regardless of the value of θ . Consequently, the TE modes (TM) may be delocalized in such a case and delocalization should not be interpreted as a Brewster anomaly as, although ω_j is finite, it is independent of θ . As in the limits $\omega \rightarrow 0$ and $\omega \rightarrow \infty$ analyzed above, delocalization would be omnidirectional at this frequency value. If the remaining positive real zeros of ω satisfying equation $g_O^X(\omega, \theta) = 0$ ($X = \text{TE}$ or $X = \text{TM}$) also satisfy condition (7), then they may be identified as the usual Brewster anomalies obtained for a given value of the incidence angle.

III. RESULTS AND DISCUSSION

A. RHM-RHM nondispersive systems

We, first, consider slabs A and B composed of two different nondispersive materials, for which both magnetic permeabilities and electric permittivities are positive and independent of the wave frequency. For normal incidence one may see that, if $Z_A^2 = Z_B^2$, then the localization length diverges for all values of the wave frequency, as expected.²² One may note that if condition $Z_A^2 \neq Z_B^2$ is satisfied, there is only one value of the critical frequency, $\omega_c = 0$. Furthermore, according to Eq. (4) and Eqs. (9)–(11), it is possible to show that

$$\xi \xrightarrow{\lambda \rightarrow \infty} \frac{2}{\pi^2} \frac{\bar{\epsilon} \bar{\mu}}{[\epsilon_A \mu_B - \epsilon_B \mu_A]^2} \frac{d^5}{\sigma_A^2 b^2 + \sigma_B^2 a^2} \left(\frac{\lambda}{d} \right)^2, \quad (18)$$

where $\bar{\epsilon} = (\epsilon_A a + \epsilon_B b)/d$ and $\bar{\mu} = (\mu_A a + \mu_B b)/d$. We note that the λ^2 asymptotic behavior of the localization length as $\lambda \rightarrow \infty$ is a well-known result already reported for RHM-RHM nondispersive multilayered systems.²²

To compare the analytical predictions for the localization length obtained from the I-M equation with the numerical results calculated from Eq. (1), we display in Fig. 1, for normal incidence, the localization length, as a function of the vacuum wavelength, in a RHM-RHM multilayered system of $N = 10^6$ double layers, with the localization length expressed in units of the average system length $\langle L \rangle = Nd$. For simplicity, we have used the same disorder amplitude for both slabs A and B , i.e., $\Delta_A = \Delta_B = \Delta$. Calculations were performed for $a = b = 12 \mu\text{m}$, and we have chosen the electric permittivities and magnetic permeabilities as in an air-silicon stack ($\epsilon_A = \mu_A = \mu_B = 1$ and $\epsilon_B = 13.18$ ²⁷). Solid lines in Figs. 1(a) and 1(b) correspond to the localization length obtained from the I-M equation for $\Delta = 1 \mu\text{m}$ and $\Delta = 12 \mu\text{m}$, respectively, whereas circles and squares are the numerical results obtained from Eq. (1) also for $\Delta = 1 \mu\text{m}$ and $\Delta = 12 \mu\text{m}$, respectively, and for 100 realizations of disorder. In addition, we have displayed the λ^2 asymptotic behavior of the localization length evaluated by using Eq. (18) (cf. oblique dashed-dotted lines in Fig. 1). Notice that, in contrast with the I-M results, the localization

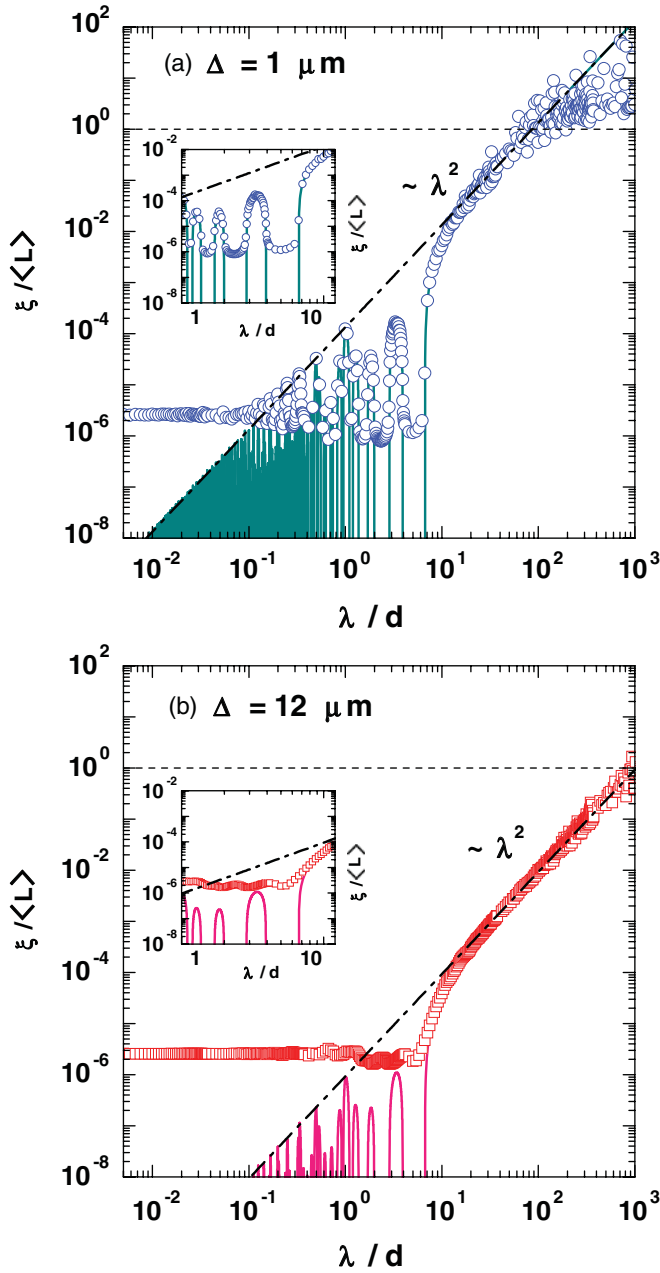


FIG. 1. (Color online) Localization length for normal incidence, in units of the average system length $\langle L \rangle$, as a function of the vacuum wavelength (expressed in units of $d = a + b$) in a RHM-RHM multilayered system of $N = 10^6$ double layers, with $a = b = 12 \mu\text{m}$, $\epsilon_A = \mu_A = \mu_B = 1$, and $\epsilon_B = 13.18$. Circles and squares correspond to numerical results obtained from Eq. (1) for $\Delta = 1 \mu\text{m}$ and $\Delta = 12 \mu\text{m}$, respectively, and for 100 realizations of disorder. In panels (a) and (b), solid curves correspond to calculations obtained from Eq. (2) for $\Delta = 1 \mu\text{m}$ and $\Delta = 12 \mu\text{m}$, respectively, and oblique dashed-dotted lines depict the λ^2 asymptotic behavior from Eq. (18), for $\Delta = 1 \mu\text{m}$ and $\Delta = 12 \mu\text{m}$, respectively. The horizontal dashed lines separate localized and delocalized states. Results are also depicted in the insets for a narrow window of vacuum wavelengths.

length obtained from Eq. (1) remains constant in the limit $\lambda \rightarrow 0$. A similar result was reported by Asatryan *et al.*^{13,14} Discrepancies are essentially due to the inapplicability of the I-M equation at the short wavelength (or high-frequency) limit in

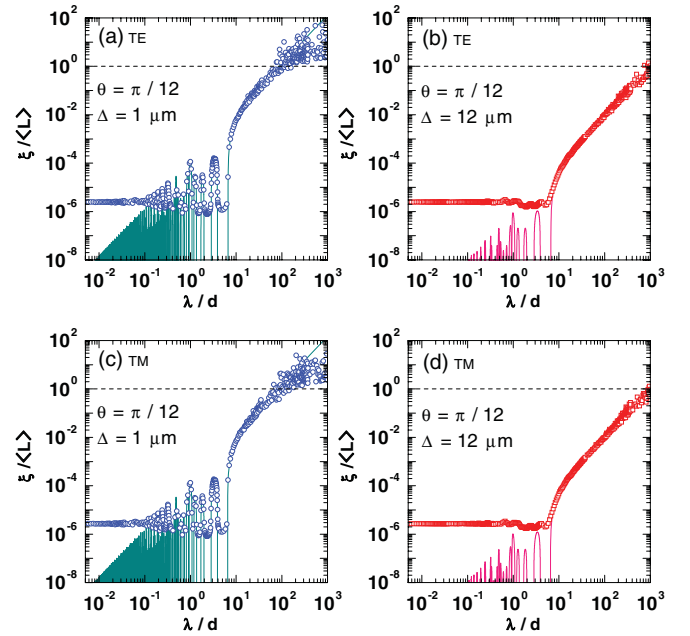


FIG. 2. (Color online) As in Fig. 1, for oblique incidence (with incidence angle $\theta = \pi/12$). Results were obtained for the TE [panels (a) and (b)] and TM [panels (c) and (d)] modes.

nondispersive superlattices. In this limit the condition $Q_x^2 \sigma_x^2 \ll 1$ ($x = A, B$), under which the I-M equation was obtained, is not fulfilled. In the long wavelength limit the I-M equation leads to $\xi \propto \lambda^2$. Numerical calculations obtained from Eq. (1) also display such behavior of ξ in that limit. As $Q_x^2 \sigma_x^2 \rightarrow 0$ ($x = A, B$) as $\lambda \rightarrow \infty$, one may expect a good agreement between the theoretical model and numerical calculations in such a wavelength region. However, for the larger values of λ and for low disorder amplitudes [cf. Fig. 1(a)] one may observe a slight dispersion of the numerical results around the λ^2 curve. This behavior is essentially due to the finiteness of the system length, which artificially affects the numerical results obtained from Eq. (1) mainly in the case of $\Delta \ll d$, where the localization length is greater than that obtained for $\Delta \sim d$. One may note from Fig. 1(b) that, for larger disorder amplitude, the λ^2 prediction derived from the I-M equation is in good agreement with numerical results computed from Eq. (1). On the other hand, for intermediate wavelengths, the I-M results and numerical calculations agree only for the smallest value of the disorder amplitude (cf. the insets of Fig. 1). A similar situation takes place for oblique incidence, as one may clearly see from Fig. 2, where the localization lengths corresponding to TE and TM polarizations are depicted as functions of λ .

It is apparent from Figs. 1 and 2 that the I-M equation describes very well the frequency dependence of the localization length for intermediate wavelengths and in the limit $\lambda \rightarrow \infty$. In the limit $\lambda \rightarrow 0$, however, the localization length remains independent of the wavelength (or frequency), and the I-M model is not applicable.

B. RHM-LHM superlattices with dispersive Drude responses

Let us now consider RHM-LHM multilayered systems in which layers A are nondispersive RHMs and layers B

TABLE I. Conditions for which ω_c [cf. Eq. (21)] is a critical frequency, obtained for photonic systems composed by layers A of a nondispersive RHM and LHM layers B with dispersive electric permittivity and magnetic permeability given by a Drude-like model.

Case 1	ω_m	$<$	$\omega_e Z_A/Z_\infty$	and	Z_∞	$<$	Z_A
Case 2	ω_m	$>$	$\omega_e Z_A/Z_\infty$	and	Z_∞	$>$	Z_A
Case 3	ω_m	$=$	$\omega_e Z_A/Z_\infty$	and	Z_∞	\neq	Z_A
Case 4	ω_m	\neq	$\omega_e Z_A/Z_\infty$	and	Z_∞	$=$	Z_A

consist of dispersive LHMs with both electric permittivity and magnetic permeability given by the Drude model,^{28,29} i.e.,

$$\epsilon_B(\omega) = \epsilon_\infty \left(1 - \frac{\omega_e^2}{\omega^2}\right) \quad (19)$$

and

$$\mu_B(\omega) = \mu_\infty \left(1 - \frac{\omega_m^2}{\omega^2}\right), \quad (20)$$

where ω_e and ω_m are the electric and magnetic plasmon frequencies, respectively, and ϵ_∞ and μ_∞ are the positive electric permittivity and magnetic permeability, respectively, of material B in the limit $\omega \rightarrow \infty$.

Let us, first, consider the case of normal incidence. By defining $Z_\infty = \sqrt{\mu_\infty}/\sqrt{\epsilon_\infty}$ as the optical impedance of the layers B at infinite frequency, it may be shown that the critical frequency is given by

$$\omega_c = \sqrt{\frac{\omega_m^2 - \omega_e^2 Z_A^2/Z_\infty^2}{1 - Z_A^2/Z_\infty^2}} \quad (21)$$

under any of the conditions summarized in Table I. Each of such conditions guarantees a real value of ω_c and an optical impedance $Z(\omega_c)$ independent on the growth-direction coordinate. One may note that, if $\omega_m = \omega_e Z_A/Z_\infty$ and, simultaneously, $Z_A = Z_\infty$, the function g_N [cf. Eq. (10)] vanishes and ξ goes to infinity for all values of the wave frequency ω .

The first two cases shown in Table I lead to finite and nonzero values of the critical frequency, whereas the third and fourth cases lead to critical frequencies equal to zero and infinity, respectively. As a consequence of the Drude-like electric and magnetic responses given by Eqs. (19) and (20), respectively, one may note that $Q_B^2 \sigma_B^2$ diverges as $\omega \rightarrow 0$ (or $\lambda \rightarrow \infty$) and $\omega \rightarrow \infty$ (or $\lambda \rightarrow 0$), whereas $Q_A^2 \sigma_A^2$ diverges in the limit $\omega \rightarrow \infty$ ($\lambda \rightarrow 0$). It must be emphasized that, at these two limits, the I-M equation could not be applied to describe the frequency dependence of the localization length. Nevertheless, it is interesting to obtain the asymptotic behavior of the localization length as a function of the frequency (or vacuum wavelength) by taking the corresponding limits $\lambda \rightarrow \infty$ or $\lambda \rightarrow 0$ in Eq. (2). In this sense, if the third condition of Table I is satisfied, one may show, for Drude-like responses, that

$$\xi \xrightarrow{\lambda \rightarrow \infty} \sin^2 \left[\frac{2\pi}{\lambda} |\bar{n}(\lambda)| d \right] \xi_{\max}(\lambda), \quad (22)$$

where

$$\xi_{\max}(\lambda) = \Lambda_\infty \left(\frac{\lambda}{d} \right)^4, \quad (23)$$

$$\Lambda_\infty = \frac{d^5}{2\pi^4 \epsilon_A^2 \mu_\infty^2 \left(1 - \frac{Z_A^2}{Z_\infty^2}\right)^2 \sigma_B^2 a^2}, \quad (24)$$

$$|\bar{n}(\lambda)| = \frac{n_A a + |n_B(\lambda)| b}{d}, \quad (25)$$

and $|n_B(\lambda)| = |\sqrt{\epsilon_B(2\pi c/\lambda)}| |\sqrt{\mu_B(2\pi c/\lambda)}|$. It is apparent from Eq. (22) that the I-M equation predicts a rapid oscillatory behavior of the localization length in the limit $\lambda \rightarrow \infty$, provided that the third condition of Table I is fulfilled. The oscillatory part of the localization length is modulated by λ^4 , which governs the behavior of the maxima of ξ as functions of λ [cf. Eq. (23)]. The λ^4 dependence of the localization length in the long wavelength limit, which is a consequence of the Drude-like frequency dependence of both the electric permittivity and magnetic permeability of layers B [cf. Eqs. (19) and (20)], differs from the asymptotic behavior of ξ previously reported by Asatryan and coworkers^{13,14} and by Torres-Herrera *et al.*¹⁶ in photonic heterostructures made of layers with random refractive indices. We should also mention that the behavior $\xi \propto \lambda^4$ was obtained for RHM-RHM 1D disordered photonic crystals,²² in the limit $\lambda \rightarrow \infty$, by introducing a linear correlation between the fluctuations of the layer widths. Such a physical situation differs from the one studied in the present work, where no correlation between the disorder of the photonic slabs was taken into account.

If the fourth condition of Table I is satisfied, then one may obtain, for Drude-like responses, that

$$\xi \xrightarrow{\lambda \rightarrow 0} \Gamma_0 G_0(\lambda) \left(\frac{\lambda}{d} \right)^{-2}, \quad (26)$$

where

$$\Gamma_0 = \frac{32\pi^2 c^4}{\epsilon_A^2 \mu_\infty^2 d (\omega_e^2 - \omega_m^2)^2}, \quad (27)$$

$$G_0(\lambda) = \frac{\sin^2 \left[\frac{2\pi}{\lambda} \bar{n}_\infty d \right]}{\sigma_A^2 \frac{\sin^2 \left[\frac{2\pi}{\lambda} b \sqrt{\epsilon_\infty \mu_\infty} \right]}{\epsilon_\infty \mu_\infty} + \sigma_B^2 \frac{\sin^2 \left[\frac{2\pi}{\lambda} a \sqrt{\epsilon_A \mu_A} \right]}{\epsilon_A \mu_A}}, \quad (28)$$

and

$$\bar{n}_\infty = \frac{\sqrt{\epsilon_A \mu_A} a + \sqrt{\epsilon_\infty \mu_\infty} b}{d}. \quad (29)$$

The localization length may be expressed as a bounded and highly oscillatory function of λ [$\Gamma_0 G_0(\lambda)$] modulated by a power-of- λ function. Maxima of ξ are then given by

$$\xi_{\max}(\lambda) = \Lambda_0 \left(\frac{\lambda}{d} \right)^{-2}, \quad (30)$$

where $\Lambda_0 = \Gamma_0 \beta$ and β is the amplitude of the oscillations of $G_0(\lambda)$. The above-obtained theoretical results may be generalized for the case of oblique incidence, with critical frequencies obtained similarly as in Sec. II. Here we mention that Case 3 in Table I was analyzed by Mogilevtsev *et al.*¹⁷

We now compare the above theoretical I-M predictions with the numerical results obtained from Eq. (1). We have supposed the same disorder amplitude Δ for both the photonic

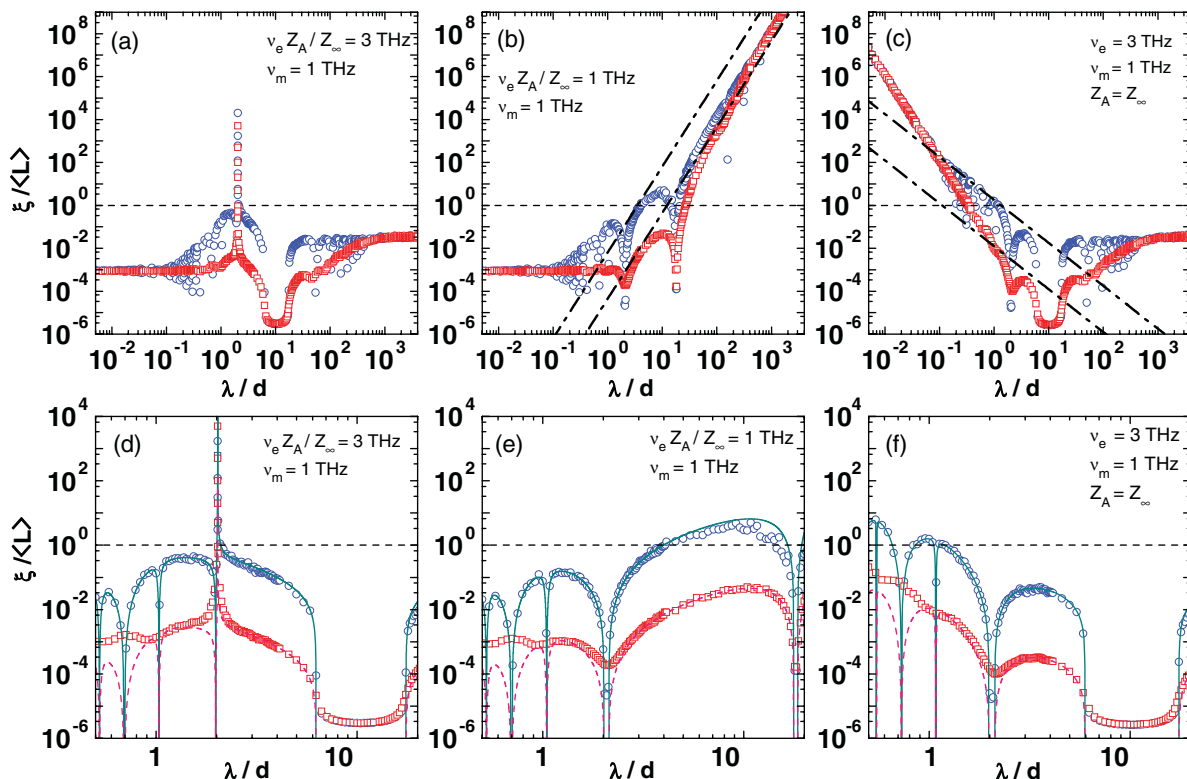


FIG. 3. (Color online) Localization length for normal incidence in units of the average system length $\langle L \rangle$ as a function of the vacuum wavelength (expressed in units of $d = a + b$) for $N = 500\,000$ double layers in a RHM-LHM photonic system with $a = b = 12\,\mu\text{m}$. Layers A are composed by a nondispersive RHM, whereas in dispersive layers B both the electric permittivity and magnetic permeability are described by a Drude-like model [cf. Eqs. (19) and (20), respectively]. Circles and squares correspond to numerical results obtained from Eq. (1) for $\Delta = 1\,\mu\text{m}$ and $\Delta = 12\,\mu\text{m}$, respectively, and for 100 realizations of disorder. Calculations displayed in (a) and (b) were performed for $\epsilon_\infty = 1.21$, $\mu_\infty = 1$, and $\epsilon_A = \mu_A = 1$ and correspond to the physical situations described in the first and third rows, respectively, of Table I. Results depicted in (c) are obtained for $\epsilon_A = \epsilon_\infty = 1.21$ and $\mu_A = \mu_\infty = 1$ and correspond to Case 4 of Table I. In all cases, the corresponding plasmon frequencies $\nu_e = \omega_e/(2\pi)$ and $\nu_m = \omega_m/(2\pi)$ are given in each panel. Upper ($\Delta = 1\,\mu\text{m}$) and lower ($\Delta = 12\,\mu\text{m}$) oblique dashed-dotted lines depicted in panels (b) and (c) correspond, respectively, to the λ^4 and λ^{-2} behaviors [cf. Eqs. (23) and (30), respectively]. Panels (d), (e), and (f) display the localization length, shown in panels (a), (b), and (c), respectively, in a short range of intermediate wavelengths, where solid and dashed curves are obtained from the I-M equation for $\Delta = 1\,\mu\text{m}$ and $\Delta = 12\,\mu\text{m}$, respectively. Horizontal dashed lines represent the separation between localized and delocalized states.

layers A and B . Numerical results for ξ , in units of the average system length, are depicted in Fig. 3 as functions of λ for normal incidence, for $N = 500\,000$ double layers in a RHM-LHM photonic system, and for $a = b = 12\,\mu\text{m}$. Circles and squares correspond to numerical results obtained from Eq. (1) for $\Delta = 1\,\mu\text{m}$ and $\Delta = 12\,\mu\text{m}$, respectively, and for 100 realizations of disorder. Calculations shown in Figs. 3(a) and 3(b) were performed for $\epsilon_\infty = 1.21$, $\mu_\infty = 1$, and $\epsilon_A = \mu_A = 1$ ($Z_\infty < Z_A$) and correspond to the physical situations described in Cases 1 and 3 of Table I, respectively. Results shown in Fig. 3(c) were obtained for $\epsilon_A = \epsilon_\infty = 1.21$ and $\mu_A = \mu_\infty = 1$ ($Z_\infty = Z_A$) and for parameters taken according to Case 4 of Table I. Upper ($\Delta = 1\,\mu\text{m}$) and lower ($\Delta = 12\,\mu\text{m}$) dashed-dotted oblique lines depicted in Figs. 3(b) and 3(c) result from the asymptotic Eqs. (23) and (30), respectively. Horizontal dashed lines represent the border between localized and delocalized states. As one may note from Fig. 3, in all cases the I-M equation correctly predicts the critical-frequency values, i.e., a non-null and finite value of ω_c (or $\lambda_c = 2\pi c/\omega_c$)

in Fig. 3(a), $\omega_c = 0$ ($\lambda_c \rightarrow \infty$) in Fig. 3(b), and an infinite value of ω_c ($\lambda_c = 0$) in Fig. 3(c).

One should note that the numerical results represented by open symbols in Fig. 3(b) follow, in the long wavelength limit, the approximated expression $\xi/\langle L \rangle = \Xi_\infty (\lambda/d)^{\alpha_\infty}$. The values of Ξ_∞ and α_∞ may be obtained for any value of the disorder amplitude by performing a statistical analysis. A detailed study of the results shown in Fig. 3(b) leads to $\Xi_\infty = (8.7 \pm 0.9) \times 10^{-5}$ and $\alpha_\infty = 4.06 \pm 0.03$ for $\Delta = 1\,\mu\text{m}$, whereas for $\Delta = 12\,\mu\text{m}$ one obtains $\Xi_\infty = (7.2 \pm 0.6) \times 10^{-5}$ and $\alpha_\infty = 4.08 \pm 0.02$. In spite that the I-M model is not strictly applicable in the long wavelength limit, it is remarkable that the values of α_∞ are found in good agreement with the λ^4 behavior predicted by Eq. (23). According to Eq. (23), the quantity equivalent to Ξ_∞ is $\Lambda_\infty/\langle L \rangle$, where Λ_∞ is given by Eq. (24). We have straightforwardly obtained that $\Lambda_\infty/\langle L \rangle = 6.4 \times 10^{-3}$ and $\Lambda_\infty/\langle L \rangle = 4.5 \times 10^{-5}$ for $\Delta = 1\,\mu\text{m}$ and $\Delta = 12\,\mu\text{m}$, respectively. It is noticeable that the quantity Ξ_∞ is not as dependent on Δ as $\Lambda_\infty/\langle L \rangle$ is. In a similar way, the

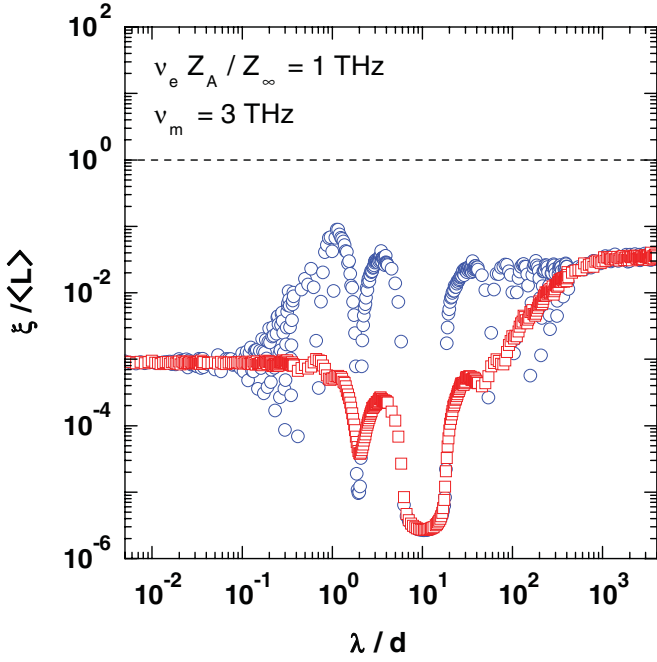


FIG. 4. (Color online) Localization length for normal incidence, as in Fig. 3 (a), for plasmon frequencies $\nu_e = \omega_e/(2\pi)$ and $\nu_m = \omega_m/(2\pi)$, which do not match any of the conditions of Table I.

numerical results of the localization length shown in Fig. 3(c) may be approximated, in the short wavelength region, by the expression $\xi/\langle L \rangle = \Xi_0 (\lambda/d)^{\alpha_0}$. In this case we found $\Xi_0 = (1.27 \pm 0.08) \times 10^{-2}$ and $\alpha_0 = -3.98 \pm 0.04$ for $\Delta = 1 \mu\text{m}$, whereas $\Xi_0 = (1.16 \pm 0.05) \times 10^{-2}$ and $\alpha_0 = -4.01 \pm 0.02$ for $\Delta = 12 \mu\text{m}$. Numerical results obtained from Eq. (1) suggest a dependence $\xi \propto \lambda^{-4}$ of the localization length in the limit $\lambda \rightarrow 0$. Such behavior differs quantitatively from the $\xi \propto \lambda^{-2}$ dependence of the localization length predicted by the I-M equation [cf. Eq. (30)], a fact which is expected due to the divergence of both $Q_A^2 \sigma_A^2$ and $Q_B^2 \sigma_B^2$ as $\lambda \rightarrow 0$ and, therefore, to the inapplicability of Eq. (2) at this limit. Even though the description, by using Eq. (2), of the asymptotic behavior of the localization length in the limits of short and long wavelength is only qualitative in this particular case, such equation correctly predicts the values of critical frequencies. On the other hand, due to the particular frequency dependence of both $\epsilon(\omega)$ and $\mu(\omega)$ [cf. Eqs. (19) and (20)], one may note that the I-M may be used without difficulties in a finite window of the wavelength spectrum. In this sense, the good agreement between the I-M results and numerical calculations from Eq. (1) may be observed in Figs. 3(d), 3(e), and 3(f).

We have depicted in Fig. 4 the localization length, for normal incidence, as a function of the vacuum wavelength. Both the electric and magnetic plasmon frequencies were chosen so that none of the conditions shown in Table I are satisfied. The rest of parameters are the same as those used in Figs. 3(a) and 3(b). One may note that $Z_\infty < Z_A$ and $\omega_m > \omega_e Z_A / Z_\infty$ in this case. According to Eq. (21), the critical frequency ω_c is an imaginary number in this case and, as expected, the suppression of the Anderson localization is not observed.

In order to consider the effects of the oblique incidence on the localization length, we have investigated whether the behavior of ξ , obtained from the conditions of Fig. 3, survives with $\theta \neq 0$. To this end, we depict in Figs. 5(a), 5(b), and 5(c) the localization length, as a function of the vacuum wavelength, calculated with the same sets of parameters as in Figs. 3(a), 3(b), and 3(c), respectively, for TE modes and incidence angle $\theta = \pi/3$. Brewster anomalies at finite values of the vacuum wavelength may be clearly observed in all panels of Fig. 5. Numerical values of such critical wavelengths (or frequencies) may be obtained by using the procedure described by Mogilevtsev *et al.*¹⁷ One may note in Figs. 5(d), 5(e), and 5(f) the very good agreement, in a segment of the applicability region of Eq. (2), between the numerical results obtained from Eq. (1) and those obtained from the I-M equation. In contrast to the case of normal incidence in which Case 3 of Table I is satisfied [cf. Fig. 3(b)], the localization length does not diverge in the limit $\lambda \rightarrow \infty$ when $\theta = \pi/3$ [cf. Fig. 5(b)]. Numerical results depicted in Fig. 5(b) indicate that the asymptotic behavior of ξ in the long wavelength limit is not robust for oblique incidence, i.e., it is strongly dependent on the incidence angle θ . Here we note that, when Case 4 of Table I is fulfilled, the diverging behavior of the localization length in the limit $\lambda \rightarrow 0$ still survives for oblique incidence, as one may note in Fig. 5(c). This particular situation is due to the choice of $\mu_A = \mu_\infty = 1$ in the numerical calculations, as we have mentioned in Sec. II. As a consequence, the function g_O^{TE} becomes independent of θ in the short wavelength limit which, together with the condition $Z_A = Z_\infty$, leads to $g_O^{\text{TE}} = 0$ as $\lambda \rightarrow 0$ and, therefore, to the suppression of the Anderson localization at this limit.

C. RHM-LHM superlattices with dispersive SRR responses

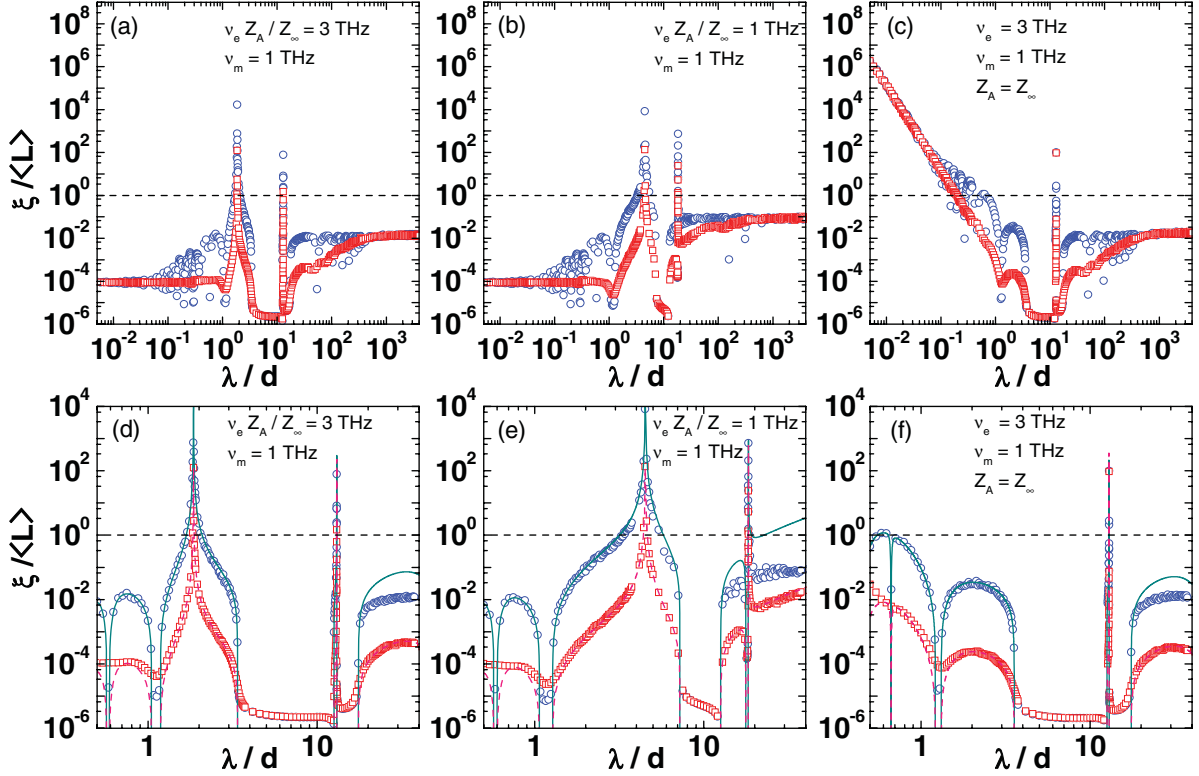
Numerical results for the localization length in the long wavelength limit may not be reliable when the Drude-like model is used for the magnetic response of the metamaterial layers B . A more realistic model for describing the frequency dependence of the magnetic permeability of the slabs B is, therefore, advisable in order to study photonic-crystal properties in the low-frequency limit. We have then considered a split-ring resonator (SRR) response for the metamaterial slabs B , where the electric permittivity is still given by the Drude model [cf. Eq. (19)] and the magnetic permeability has the form³⁰⁻³²

$$\mu_B(\omega) = \mu_0 \left(1 - F \frac{\omega^2}{\omega^2 - \omega_m^2} \right), \quad (31)$$

where $0 < F < 1$ is a factor which depends on the geometry of the split rings³¹ and ω_m plays the role of a magnetic-resonance frequency.

We now proceed, as in the above subsection, to find the critical frequencies from the I-M equation. For normal incidence the critical frequencies come from the condition $g_N(\omega_c) = 0$ and, therefore, are the real and positive solutions of the equation

$$\left(\frac{Z_\infty^2}{Z_A^2} - 1 \right) \omega_c^4 + \left[\omega_e^2 + \omega_m^2 \left(1 - \frac{Z_\infty^2}{Z_A^2} \frac{1}{1-F} \right) \right] \omega_c^2 - \omega_e^2 \omega_m^2 = 0, \quad (32)$$

FIG. 5. (Color online) As in Fig. 3 but for TE modes and oblique incidence ($\theta = \pi/3$).

where $Z_A = \sqrt{\mu_A}/\sqrt{\epsilon_A}$ is the optical impedance of slabs A and $Z_\infty = \sqrt{\mu_\infty}/\sqrt{\epsilon_\infty}$ is the optical impedance of meta-material layers B in the limit $\omega \rightarrow \infty$. Here we note that $\mu_\infty = \mu_0(1 - F)$ is the high-frequency magnetic permeability of slabs B . The above equation, together with Eqs. (9)–(11), indicates that $\omega = 0$ is not a critical frequency and, therefore, we find localized states in the long wavelength limit.

For simplicity, we have studied the two particular cases of Eq. (32) which have been summarized in Table II. In Case 1 we have supposed $Z_\infty = Z_A$, and as a consequence, the fourth-order term in ω_c of Eq. (32) vanishes. One has $\omega_e > \omega_m \sqrt{\frac{F}{1-F}}$ in order to obtain real solutions for ω_c . The critical frequency

is then given by

$$\omega_c = \frac{\omega_e \omega_m}{\sqrt{\omega_e^2 - \omega_m^2 \frac{F}{1-F}}}. \quad (33)$$

Also, due to the matching of the optical impedance of slabs A and B when $\omega \rightarrow \infty$, one may expect the suppression of Anderson localization in such a limit. In this case, the behavior of the localization length, predicted from the I-M equation, is described by Eq. (26), where

$$\Gamma_0 = \frac{32 \pi^2 c^4}{\epsilon_A^2 \mu_\infty^2 d (\omega_e^2 - \omega_m^2 \frac{F}{1-F})^2} \quad (34)$$

and $G_0 = G_0(\lambda)$ is given by Eq. (28), with $\mu_\infty = \mu_0(1 - F)$ in Eq. (29). The function modulating the maxima of ξ is given by Eq. (30), with the appropriate value of Λ_0 obtained from Γ_0 and G_0 , as we have mentioned in the above subsection.

In Case 2 of Table II, we have imposed the condition $\omega_e = \omega_m \sqrt{\frac{Z_\infty^2}{Z_A^2(1-F)}} - 1$, with $Z_\infty > Z_A \sqrt{1-F}$ in order to ω_e be real. As a consequence, the quadratic term in ω_c of Eq. (32) vanishes, and $Z_\infty > Z_A$ for obtaining real values of the critical frequency. We have discarded the two imaginary solutions and the negative real solution of Eq. (32), as none of them has a physical meaning. The single positive solution for ω_c reads,

$$\omega_c = \frac{\sqrt{\omega_e \omega_m}}{\sqrt[4]{\frac{Z_\infty^2}{Z_A^2} - 1}}. \quad (35)$$

We have numerically obtained the localization length from Eq. (1) and compared it with the theoretical predictions resulting from the I-M equation. We have supposed the same

TABLE II. Two particular cases of Eq. (32). Conditions imposed to Eq. (32) guarantees the suppression of Anderson localization, for normal incidence, at the critical frequencies shown in the right column. The photonic system is composed by layers A of a nondispersive RHM, and by layers B of a SRR metamaterial with electric permittivity and magnetic permeability given by Eqs. (19) and (31), respectively.

Cases	Conditions	Critical frequency
1	$\omega_e > \omega_m \sqrt{\frac{F}{1-F}}$ $Z_\infty = Z_A$	$\omega_c \rightarrow \infty$ $\omega_c = \frac{\omega_e \omega_m}{\sqrt{\omega_e^2 - \omega_m^2 \frac{F}{1-F}}}$
2	$\omega_e = \omega_m \sqrt{\frac{Z_\infty^2}{Z_A^2(1-F)}} - 1$ $Z_\infty > Z_A$	$\omega_c = \frac{\sqrt{\omega_e \omega_m}}{\sqrt[4]{\frac{Z_\infty^2}{Z_A^2} - 1}}$

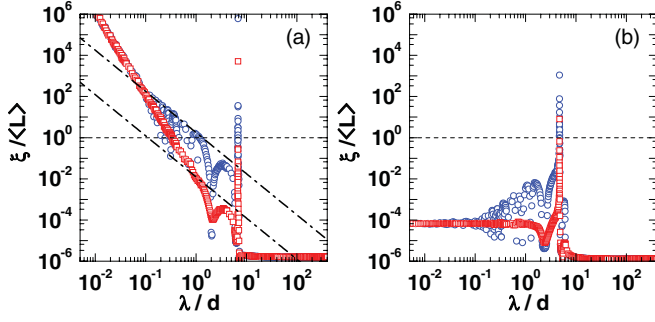


FIG. 6. (Color online) Localization length, for normal incidence, in units of the average system length $\langle L \rangle$, as a function of the vacuum wavelength expressed in units of $d = a + b$. Calculations were performed using Eq. (1), $a = b = 12 \mu\text{m}$, $N = 500\,000$, and 100 realizations of disorder. Circles and squares correspond to numerical data obtained for $\Delta = 1 \mu\text{m}$ and $\Delta = 12 \mu\text{m}$, respectively. The electric and magnetic responses of layers B are described by Eqs. (19) and (31), respectively, with $\epsilon_A = \epsilon_\infty = 1.21$, $\mu_A = 1$, $F = 1/4$, and $\frac{\omega_e}{2\pi} = 3 \text{ THz}$. Results displayed in (a) were computed by setting $\mu_0 = 4/3$ and $\frac{\omega_m}{2\pi} \sqrt{\frac{F}{1-F}} = 1 \text{ THz}$ and correspond to Case 1 of Table II.

Parameters used in (b) were $\mu_0 = 8/3$ and $\frac{\omega_m}{2\pi} \sqrt{\frac{Z_\infty^2}{Z_A^2} \frac{1}{1-F}} - 1 = 3 \text{ THz}$ and correspond to Case 2 of Table II. Upper and lower oblique lines in panel (a) correspond to the asymptotic behavior of the localization length, for $\Delta = 1 \mu\text{m}$ and $\Delta = 12 \mu\text{m}$, respectively, obtained as explained in the text. Horizontal dashed lines represent the separation between localized and delocalized states.

disorder amplitude for both slabs A and B . Figure 6 shows the normal-incidence localization length in a multilayered system with the electric and magnetic dispersions of slabs B given by Eqs. (19) and (31), respectively. Results depicted in Figs. 6(a) and 6(b) are obtained by appropriately choosing the superlattice parameters according to Cases 1 and 2, respectively, of Table II. Circles and squares correspond to $\Delta = 1 \mu\text{m}$ and $\Delta = 12 \mu\text{m}$, respectively. As in the previous subsection, the localization length may be written, in the vicinity of $\lambda = 0$, as $\xi/\langle L \rangle = \Xi_0 (\lambda/d)^{\alpha_0}$. A statistical analysis of the numerical data obtained from Eq. (1) reveals that $\Xi_0 = (1.34 \pm 0.07) \times 10^{-2}$ and $\alpha_0 = -3.98 \pm 0.03$ for $\Delta = 1 \mu\text{m}$, whereas $\Xi_0 = (1.08 \pm 0.04) \times 10^{-2}$ and $\alpha_0 = -4.03 \pm 0.02$ for $\Delta = 12 \mu\text{m}$. Such results are in agreement with those previously obtained for the Drude-like response in metamaterial layers B and suggest a dependence $\xi \propto \lambda^{-4}$ in the limit $\lambda \rightarrow 0$. The I-M equation correctly predicts the singularity of the localization length as $\lambda \rightarrow 0$, but such a prediction is only qualitative. For finite values of the critical frequency, however, the I-M equation quantitatively predicts the position of the peaks displayed in both Figs. 6(a) and 6(b). The corresponding vacuum wavelength ($\lambda_c = 2\pi c/\omega_c$) associated with those critical frequencies are $\lambda_c/d \approx 6.80$ and $\lambda_c/d \approx 4.73$, respectively, and agree very well with the results obtained from Eqs. (33) and (35), respectively.

We have also numerically studied the influence of oblique incidence on the localization length. Results computed from Eq. (1) are displayed in Fig. 7. In panels 7(a) and 7(b) we have used the same set of parameters of Fig. 6(a), whereas in panels 7(c) and 7(d) the corresponding parameters were

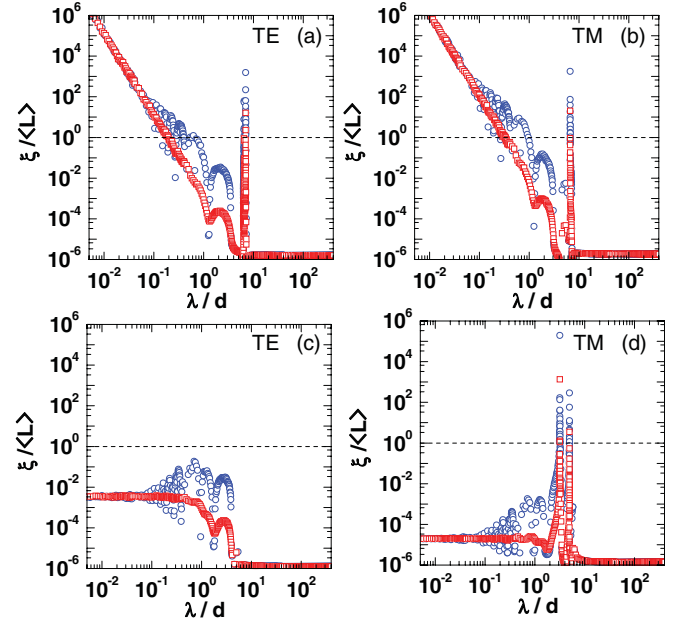


FIG. 7. (Color online) TE and TM localization lengths, in units of the average system length $\langle L \rangle$, for oblique incidence with $\theta = \pi/3$. Results depicted in (a) and (b) were performed for the same set of parameters used in Fig. 6(a), whereas the data plotted in (c) and (d) are evaluated using the parameters of Fig. 6(b). Horizontal dashed lines represent the separation between localized and delocalized states.

chosen as in Fig. 6(b). Calculations shown in Figs. 7(a) and 7(c) [7(b) and 7(d)] were obtained for TE (TM) modes. It is apparent from Figs. 7(a) and 7(b) that the singularity of ξ in the limit $\lambda \rightarrow 0$ still survives in the case of oblique incidence for both the TE and TM modes. As discussed above, these facts are due to the choice of $\mu_A = \mu_\infty = \mu_0(1 - F)$ and $\epsilon_A = \epsilon_\infty$ together with the matching of the optical impedances of the slabs A and B in the high-frequency limit. In other words, the delocalization in the limit $\lambda \rightarrow 0$ is omnidirectional for the photonic superlattice studied in Figs. 6(a), 7(a), and 7(b). Moreover, all the singularities of the localization length appearing for positive finite values of λ correspond to Brewster anomalies. As one may note from Fig. 7(c) for TE modes, the oblique incidence may lead to a situation in which no suppression of the Anderson localization is observed in the whole range of wavelengths considered in the present study. As mentioned before, the positions of the singularities of ξ in the frequency (or wavelength) spectrum for both TE and TM modes in the case of oblique incidence may be fully understood by analyzing the functions g_O^{TE} and g_O^{TM} , respectively [cf. Eqs. (15) and (16), respectively], which are displayed in Fig. 8 for the different cases depicted in Fig. 7. For example, for the TE modes shown in Fig. 7(a) the corresponding function g_O^{TE} , represented as a solid line in Fig. 8(a), vanishes at $\lambda_c/d = 0$, $\lambda_c/d \approx 6.525$, and $\lambda_c/d \approx 7.007$. The two last values of λ_c are a doublet which is observed in Fig. 7(a), due to the scale of the figure, as a single peak in the localization length. For the TM modes in Fig. 7(b) we have two singularities corresponding to the zeros of g_O^{TM} [cf. dashed line in Fig. 8(a)] located at $\lambda_c/d = 0$ and $\lambda_c/d \approx 6.679$. In the same way, one may note that the function g_O^{TE}

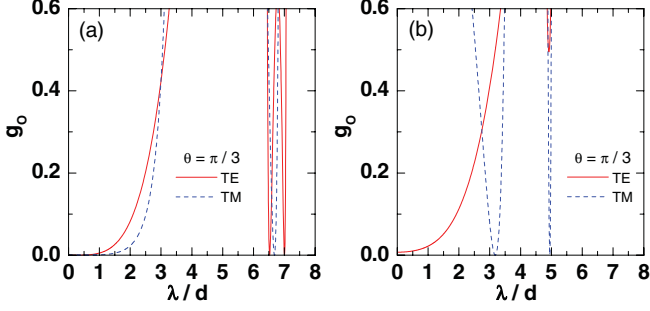


FIG. 8. (Color online) Vacuum wavelength dependence of functions g_O^X for $\theta = \pi/3$. Solid and dashed lines correspond to $X = \text{TE}$ and $X = \text{TM}$ electromagnetic modes, respectively [cf. Eqs. (15) and (16), respectively]. Results displayed in panel (a) correspond to the first case of Table II with parameters used in Figs. 7(a) and 7(b), whereas in panel (b) we use the set of parameters of Figs. 7(c) and 7(d), which correspond to the second case of Table II.

[see the solid line in Fig. 8(b)], corresponding to the TE modes displayed in Fig. 7(c), does not vanish at $\lambda = 0$ or at other values of λ and, therefore, the TE modes remain localized in this case. Also, the TM modes displayed in Fig. 7(d) are delocalized at $\lambda_c/d \approx 3.179$ and $\lambda_c/d \approx 4.948$, which are the zeros of the corresponding function g_O^{TM} [cf. dashed line in Fig. 8(b)].

D. Absorption effects

As metamaterials are intrinsically dispersive materials, it is also convenient to investigate the effects of absorption on the localization length. Such effects may be appropriately introduced by modifying the electric and magnetic responses of the heterostructure slabs. Here we assume that slabs *A* are nondispersive, whereas the electric susceptibility of slabs *B* is given by

$$\epsilon_B(\omega) = \epsilon_\infty \left[1 - \frac{\omega_e^2}{\omega(\omega + i\omega_e\gamma_e)} \right], \quad (36)$$

where γ_e is a phenomenological electric damping constant expressed in units of the electric plasmon frequency. Within the Drude-like model the magnetic permeability of the slabs

B is given by

$$\mu_B(\omega) = \mu_\infty \left[1 - \frac{\omega_m^2}{\omega(\omega + i\omega_m\gamma_m)} \right], \quad (37)$$

where γ_m is the magnetic damping constant in units of the magnetic plasmon frequency. Numerical calculations for the localization length may then be obtained from Eq. (1).

To illustrate absorption effects on ξ , we depict in Fig. 9 the localization length for normal incidence, as a function of λ , and for various values of the electric and magnetic damping constants. Calculations displayed in Figs. 9(a), 9(b), and 9(c) were performed for the same set of parameters used in Figs. 3(a), 3(b), and 3(c), respectively. Here we have restricted the range of λ to a vicinity of the critical frequencies. It is apparent from Fig. 9(a) that the Brewster anomaly, obtained in the absence of absorption, becomes smeared out as the damping constants increase. This is related to the decrease of the intensity of the transmitted beam due to the absorption in the metamaterial layers. Moreover, the asymptotic behavior of the localization length in the limit $\lambda \rightarrow \infty$ observed in Fig. 9(b) for $\gamma_e = \gamma_m = 0$ is dramatically modified in the presence of the absorption. In this case, numerical calculations indicate that the λ^4 behavior of ξ does not survive when the damping constants are introduced. Results in Fig. 9(c), however, indicate that the divergence of ξ in the limit $\lambda \rightarrow 0$ still remains in the presence of absorption.

IV. CONCLUSIONS

Summing up, we have investigated the localization properties of electromagnetic waves in 1D disordered photonic superlattices in which the electric permittivity and magnetic permeability of the different slabs composing the heterostructure may depend on the wave frequency. First, we have performed a theoretical study of the properties of the localization length by using the I-M model recently developed for weakly disordered photonic systems.^{17,22} In addition, we carried out numerical calculations of the localization length by using its definition [cf. Eq. (1)] involving the transmissivity of the heterostructure. Generally speaking, the I-M results for the localization length agree with the numerical results obtained from Eq. (1) only for small amplitudes of disorder, and in a

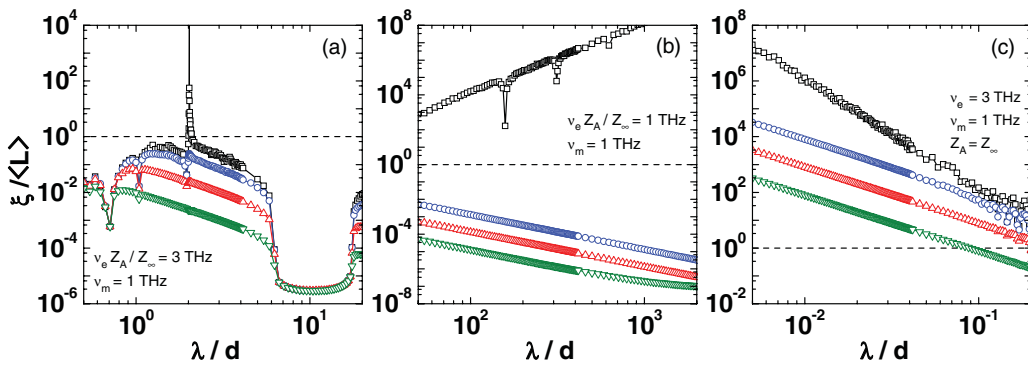


FIG. 9. (Color online) As in Fig. 3, with $\Delta = 1 \mu\text{m}$, and including effects of the absorption on the localization length. Results were displayed in the vicinity of a critical frequency. Squares, circles, up-triangles, and down-triangles correspond to damping constants $\gamma_e = \gamma_m = 0$, $\gamma_e = \gamma_m = 10^{-4}$, $\gamma_e = \gamma_m = 10^{-3}$, and $\gamma_e = \gamma_m = 10^{-2}$, respectively. Horizontal dashed lines represent the border between localized and delocalized states.

region of the frequency spectrum where the I-M model is valid. Such a region is determined by the frequency dependence of both the electric permittivity and magnetic permeability of the materials composing the heterostructure. In all cases studied in the present work, the I-M equation correctly predicts the critical-frequency values at which the localization length diverges and suppression of Anderson localization occurs.

For nondispersive RHM-RHM superlattices, present numerical results confirm the λ^2 dependence of the localization length ξ in the long wavelength limit, whereas for LHM-RHM photonic crystals we have shown that the asymptotic behavior of the localization length is strongly dependent on both electric and magnetic responses that characterize the LHM slabs, i.e., it is essentially determined by the specific type of metamaterial which constitutes the LHM layers. In this sense, results obtained from Eq. (1) suggest, under certain conditions discussed in Sec. III, a λ^4 dependence of the localization length, only for normal incidence, in the limit $\lambda \rightarrow \infty$. Moreover, in some specific cases the localization length exhibits a λ^{-4} asymptotic behavior as $\lambda \rightarrow 0$, which is

observed for both normal and oblique incidence and even in the presence of absorption.

Here, one should point out that researchers worldwide are making efforts to develop fabrication techniques that compensate losses to produce more efficient photonic media.³³ Therefore, the combination of metamaterials with electrically and optically pumped gain media and emerging graphene technology is expected to lead to low-loss materials suitable to use in optical devices and in the electronics industry. In that respect, we do hope the present theoretical study will help to stimulate low-loss experimental studies and further experimental and theoretical work on the subject of suppression of Anderson localization in disordered photonic heterostructures.

ACKNOWLEDGMENTS

The present work was partially financed by Brazilian Agencies CNPq and FAPESP as well as by the Scientific Colombian Agency CODI, University of Antioquia.

- ¹P. W. Anderson, *Phys. Rev.* **109**, 1492 (1958).
- ²A. Lagendijk, B. A. van Tiggelen, and D. S. Wiersma, *Phys. Today* **62**, 24 (2009).
- ³S. John, *Phys. Rev. Lett.* **58**, 2486 (1987).
- ⁴S. F. Liew and H. Cao, *J. Opt.* **12**, 024011 (2010).
- ⁵J. D. Joannopoulos, S. G. Johnson, J. N. Winn, and R. D. Meade, in *Photonic Crystals: Molding the Flow of Light* (Princeton University Press, Princeton, 2008).
- ⁶D. R. Smith, W. J. Padilla, D. C. Vier, S. C. Nemat-Nasser, and S. Schultz, *Phys. Rev. Lett.* **84**, 4184 (2000).
- ⁷P. Markoš and C. M. Soukoulis, *Wave Propagation: From Electrons to Photonic Crystals and Left-Handed Materials* (Princeton University Press, Princeton, 2008).
- ⁸C. Enkrich, M. Wegener, S. Linden, S. Burger, L. Zschiedrich, F. Schmidt, J. F. Zhou, Th. Koschny, and C. M. Soukoulis, *Phys. Rev. Lett.* **95**, 203901 (2005).
- ⁹W. Cai, U. K. Chettiar, H. K. Yuan, V. C. de Silva, A. V. Kildishev, V. P. Drachev, and V. M. Shalaev, *Opt. Express* **15**, 3333 (2007).
- ¹⁰D. R. Smith, J. B. Pendry, and M. C. K. Wiltshire, *Science* **305**, 788 (2004).
- ¹¹J. B. Pendry, D. Shurig, and D. R. Smith, *Science* **312**, 1780 (2006).
- ¹²U. Leonhardt, *Science* **312**, 1777 (2006).
- ¹³A. A. Asatryan, L. C. Botten, M. A. Byrne, V. D. Freilikher, S. A. Gredekskul, I. V. Shadrivov, R. C. McPhedran, and Y. S. Kivshar, *Phys. Rev. Lett.* **99**, 193902 (2007).
- ¹⁴A. A. Asatryan, S. A. Gredekskul, L. C. Botten, M. A. Byrne, V. D. Freilikher, I. V. Shadrivov, R. C. McPhedran, and Y. S. Kivshar, *Phys. Rev. B* **81**, 075124 (2010).
- ¹⁵P. Sheng, *Introduction to Wave Scattering, Localization, and Mesoscopic Phenomena* (Academic, New York, 1995).
- ¹⁶E. J. Torres-Herrera, F. M. Izrailev, and N. M. Makarov, *Europhys. Lett.* **98**, 27003 (2012).
- ¹⁷D. Mogilevtsev, F. A. Pinheiro, R. R. dos Santos, S. B. Cavalcanti, and L. E. Oliveira, *Phys. Rev. B* **82**, 081105(R) (2010).
- ¹⁸D. Mogilevtsev, F. A. Pinheiro, R. R. dos Santos, S. B. Cavalcanti, and L. E. Oliveira, *Phys. Rev. B* **84**, 094204 (2011).
- ¹⁹E. Reyes-Gómez, A. Bruno-Alfonso, S. B. Cavalcanti, and L. E. Oliveira, *Phys. Rev. E* **84**, 036604 (2011).
- ²⁰A. A. Asatryan, L. C. Botten, M. A. Byrne, V. D. Freilikher, S. A. Gredekskul, I. V. Shadrivov, R. C. McPhedran, and Y. S. Kivshar, *Phys. Rev. B* **85**, 045122 (2012).
- ²¹J. E. Sipe, P. Sheng, B. S. White, and M. H. Cohen, *Phys. Rev. Lett.* **60**, 108 (1988).
- ²²F. M. Izrailev and N. M. Makarov, *Phys. Rev. Lett.* **102**, 203901 (2009).
- ²³M. M. Sigalas, C. M. Soukoulis, C. T. Chan, R. Biswas, and K. M. Ho, *Phys. Rev. B* **59**, 12767 (1999).
- ²⁴L. I. Deych, D. Zaslavsky, and A. A. Lisyansky, *Phys. Rev. Lett.* **81**, 5390 (1998).
- ²⁵Cheng-Ching Wang, and Pi-Gang Luan, *Phys. Rev. E* **65**, 066602 (2002).
- ²⁶M. Mazilu and K. Dholakia, *Opt. Express* **14**, 7709 (2006).
- ²⁷Sadao Adachi, *J. Appl. Phys.* **58**, 1R (1985).
- ²⁸H. Jiang, H. Chen, H. Li, Y. Zhang, and S. Zhu, *Appl. Phys. Lett.* **83**, 5386 (2003), and references therein.
- ²⁹L. H. Zhang, Y. H. Lia, Y. Q. Ding, W. Tan, H. T. Jiang, Z. G. Wang, H. Q. Li, Y. W. Zhang, and H. Chen, *Eur. Phys. J. B* **77**, 1 (2010).
- ³⁰T. J. Yen, W. J. Padilla, N. Fang, D. C. Vier, D. R. Smith, J. B. Pendry, D. N. Basov, and X. Zhang, *Science* **303**, 1494 (2004).
- ³¹F. S. S. Rosa, D. A. R. Dalvit, and P. W. Milonni, *Phys. Rev. Lett.* **100**, 183602 (2008).
- ³²R. S. Penciu, M. Kafesaki, Th. Koschny, E. N. Economou, and C. M. Soukoulis, *Phys. Rev. B* **81**, 235111 (2010).
- ³³A. Fang, T. Koschny, and C. M. Soukoulis, *J. Opt.* **12**, 024013 (2010); N. I. Zheludev, *Science* **328**, 582 (2010); S. Xiao, V. P. Drachev, A. V. Kildishev, X. Ni, U. K. Chettiar, H.-K. Yuan, and V. M. Shalaev, *Nature* **466**, 735 (2010); A. Boltasseva and H. A. Atwater, *Science* **331**, 290 (2011); N. I. Zheludev, *Opt. Photon. News* **22**, 31 (2011).